Research Article

iMedPub Journals
http://www.imedpub.com

Archives in Chemical Research
ISSN 2572-4657

2017
Vol. 1 No. 1: 6

DOI: 10.21767/2572-4657.100006

Molecular Investigation and Nonlinear Optical Response of Dihydropyrimidinone: A Comparative Spectroscopic and Quantum Computational Studies

Dhandapani A[1], Adaikalaraj C[1], Manivarman S[1] and Subashchandrabose S[2]

1 PG and Research Department of Chemistry, Government Arts College, C-Mutlur, Chidambaram-608102, Tamil Nadu, India
2 Centre for Research and Development, PRIST University, Vallam, Thanjavur-613403, Tamil Nadu, India

Corresponding author:
Manivarman S

drsmgac@gmail.com

Research Department of Chemistry, Government Arts College, Tamil Nadu, India.

Tel: +91 9842483139

Citation: Dhandapani A, Adaikalaraj C, Manivarman S, et al. Molecular Investigation and Nonlinear Optical Response of Dihydropyrimidinone: A Comparative Spectroscopic and Quantum Computational Studies . Arch Chem Res. 2017, 1:1.

Abstract

Organic molecule ethyl-4-(4-chloro-3-nitrophenyl)-6-methyl-2-oxo-1,2,3,4-tetrahydropyrimidine-5-carboxylate has been synthesized. The molecular structure has been characterized using FT-IR, FT-Raman, ^{1}H and ^{13}C- NMR spectral studies. The structure of the title molecule was theoretically investigated by DFT method using B3LYP/6-31G(d,p) basis set. The firm assignments of vibrational bands are allowed using experimental and computations. The nonlinear optical property of the title molecule has been calculated using first hyperpolarizability components. The intra-molecular charge transfer occurring in the molecule have been analyzed by NBO analysis. The electronic and charge transfer properties have been studied using frontier molecular orbitals. ^{1}H and ^{13}C-NMR spectra were recorded and calculated using the gauge independent atomic orbital (GIAO) method.

Keywords: CNPC; PES; NBO; NLO; HOMO-LUMO

Received: December 01, 2016; **Accepted:** January 02, 2017; **Published:** January 09, 2017

Introduction

Organic materials are attractive due to their optical properties, electronics, and integrated photonics [1-3]. Organic molecules with electron deficient pyrimidine ring tend to act as electron acceptor and are very effectively used in Organic light emitting diodes (OLEDs) [4]. The higher light harvesting efficiency achieved by pyrimidine adopted porphyrin sensitizers show more advantage in oxidized dyes. New organic dyes with pyrimidine-2-carboxylic acid forms coordination bond with TiO_2 improves the interaction between the anchor and semiconductor [5]. Pyrimidine show considerable efforts in the development of bipolar materials to overcome the unipolar character of the organic materials [6]. Recent work from Lin et al., reported that pyrimidine used as π-conjugated spacer in organic photosensitizers in dye sensitized solar cells (DSSCs) [7]. The electron withdrawing character of pyrimidine chromophore exhibits the white photoluminescence in both liquid and solid state [8]. Moreover, pyrimidine based iridium complex exhibit external quantum efficiency up to 28.6% due to high photoluminescence quantum yield determines the excellent device performance and high efficiency [9].

In this paper, we report the synthesis, spectral and nonlinear optical investigation of ethyl-4-(4-chloro-3-nitrophenyl)-6-methyl-2-oxo-1,2,3,4-tetrahydropyrimidine-5-carboxylate (CNPC). Here the molecular structure and electronic structural properties of the title molecule were studied using experimental and also with theoretical approach. For unambiguous vibrational spectral assignments precisely potential energy distribution have been performed and related with recorded FT-IR and FT-Raman spectra, respectively. This work also covers the molecular electrostatic potential mapped surface and energy gap analysis along with global reactivity descriptors. The charge transfer interactions occur in the CNPC molecule and stabilization arising from the donor-acceptors interactions are examined using Natural bond orbital analysis. The first hyperpolarizability (β) components examining the nonlinear response of the title molecule. The NMR chemical shifts calculated using Gauge-independent atomic orbitals and experimental chemical shifts were also analyzed in the present work.

Experimental

Synthesis of ethyl 4-(4-chloro-3-nitrophenyl)-6-methyl-2-oxo-1,2,3,4-tetrahydro pyrimidine-5-carboxylate

4-Chloro-3-nitrobenzaldehyde (1.84 ml, 0.01 mmol) and urea (1.8 g, 0.03 mmol) was added to an ethanolic solution of ethyl acetoacetate (1.34 ml, 0.01 mmol). To the mixture $CeCl_3.7H_2O$ (0.465 g, 25%) was added and stirred well. Then, the reaction mixture was refluxed at 90°C for 2-3 hours and the completion of the reaction was monitored by thin layer chromatography. After completion, the reaction mixture was poured onto crushed ice and stirred up to 5-10 minutes. The solid product was separated, filtered under suction, washed with ice-cold water and then recrystallized from absolute ethanol. The synthesis of CNPC molecule is shown in **Scheme 1**. Melting point=185˚C; Yield=87%.

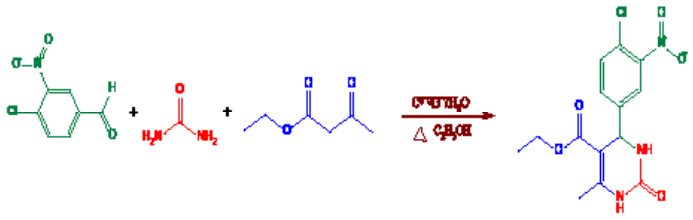

Scheme 1 The reaction scheme of synthesis of CNPC molecule.

Computational Details

The quantum chemical calculations of CNPC was performed using the B3LYP level of theory supplemented with 6-31G(d,p) basis set, using Gaussian 03 program package invoking geometry optimization [10]. Initial geometry generated from geometrical parameters was minimized without any constraint in the potential energy surface at DFT level. The optimized minimum structure parameters were used in the vibrational wavenumber calculations at the DFT level to characterize all stationary points as minima. The harmonic vibrational wavenumber calculations resulting in IR and Raman intensities and Raman depolarization ratios. The vibrational modes were assigned based on potential energy distribution analysis (PED) using VEDA4 program [11]. The Raman activities were transformed into Raman intensities using Raint program [12] by the expression:

$$I_i = 10^{-12} \times (v_o - v_i)^4 \times \frac{1}{v_i} \times RA_i$$

Where I_i is the Raman intensity, A_i is the Raman scattering activities, v_i is the wavenumber of the normal modes and v_0 denotes the wavenumber of the excitation laser [13].

Results and Discussion

Molecular conformational analysis

In order to investigate the stable conformer, potential energy surface scan was performed to CNPC molecule. In this PES scan process, the internal redundant coordinate of the dihedral angle D(C11–C13–C16–C20) chosen for the conformational flexibility within the molecule. During this scan the geometrical parameters was relaxed, while the D(C11–C13–C16–C20) torsional angle raised from 0˚ to 360˚ rotation by a step of 10˚ interval. The potential energy surface scan curve and optimized structure of CNPC is shown in **Figure 1**. From the results, there are three maximum energy conformers (0˚, 170˚ and 360˚) and two minimum conformers (100˚ and 270˚) were identified. The most stable conformer was identified at 270˚ rotation with the relative energy -1542.44631 Hartree. Hence this structure is the global minimum conformer and is used for the further investigations. The various possible conformers of CNPC during PES scan were shown in **Table 1**.

Vibrational Assignments

The detailed description of vibrational assignments of CNPC along with calculated IR/Raman intensities and potential energy distributions of the vibrations are listed in **Table 2**. For visual comparison, the recorded and simulated FT-IR and FT-Raman spectra of CNPC are shown in **Figures 2 and 3**, respectively. The un-scaled wavenumber obtained from DFT method, overestimate the observed wavenumber. To bring the theoretical wavenumber closer to the observed wavenumber, a selective scaling procedure was employed. The title molecule have 37 atoms, hence it gives 105 normal modes of vibrations, 36 stretching, 71 in-plane bending and 34 out-of-plane bending vibrations.

C-Cl vibrations

The stretching and bending vibrations of C-Cl normally occur in the low wavenumber region 760-505 cm^{-1} [14]. Vibrational couplings are possible due to lowering of the molecular symmetry and the presence of heavy atom. The C-Cl stretching vibration of CNPC is observed as strong band at 688 cm^{-1} in FT-IR spectrum along with the vibration of β_{CCC} bending vibration. The calculated wavenumber corresponds to the C-Cl stretching mode is 693 cm^{-1} with 68% of PED contribution. The chloro substituted aromatic compounds have a band of strong to medium intensity in the region 385-265 cm^{-1} due to C-Cl in-plane deformation [15]. The in-plane β_{CCCl} is observed at 338 cm^{-1} in FT-Raman spectrum with medium intensity. The calculated in-plane and out-of-plane

Table 1 The various possible conformers of CNPC.

Rotation (°)	Relative energy (Hartree)	Rotation (°)	Relative energy (Hartree)
0	-1542.442086	190	-1542.443378
10	-1542.442633	200	-1542.444049
20	-1542.443224	210	-1542.4446
30	-1542.443815	220	-1542.445019
40	-1542.444332	230	-1542.44541
50	-1542.444858	240	-1542.445776
60	-1542.44532	250	-1542.44606
70	-1542.445718	260	-1542.446271
80	-1542.445944	***270***	***-1542.446319***
90	-1542.446109	280	-1542.446277
100	-1542.44616	290	-1542.446046
110	-1542.445981	300	-1542.445461
120	-1542.445534	310	-1542.444515
130	-1542.444764	320	-1542.44338
140	-1542.443799	330	-1542.44237
150	-1542.44291	340	-1542.441835
160	-1542.442358	350	-1542.441778
170	-1542.442346	360	-1542.442086
180	-1542.442745		

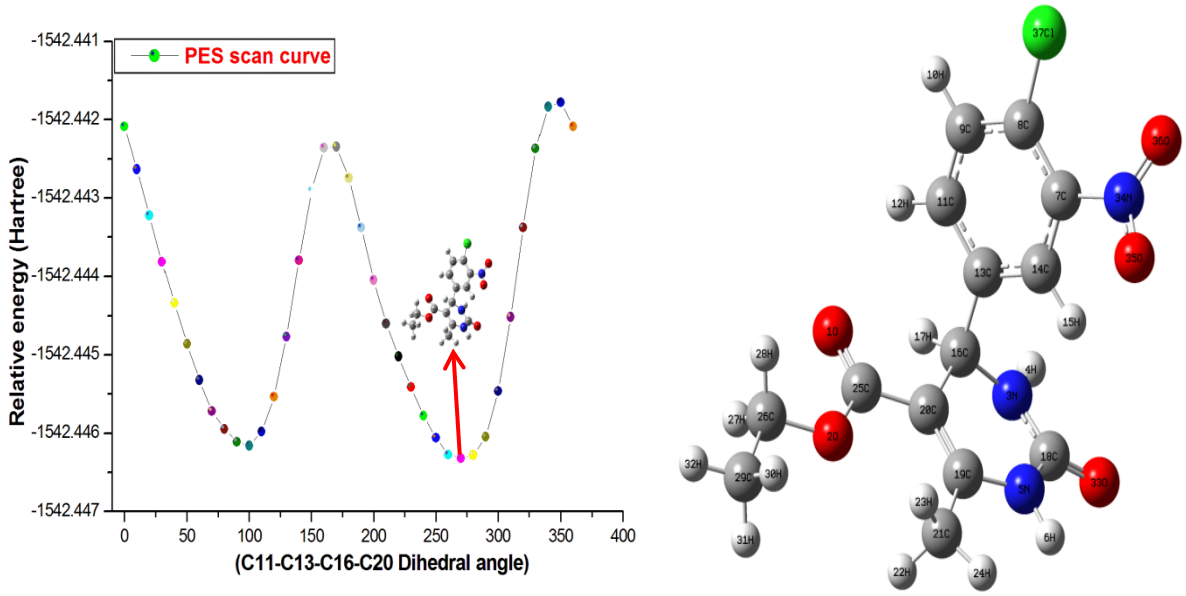

Figure 1 The potential energy surface scans curve and optimized structure of CNPC.

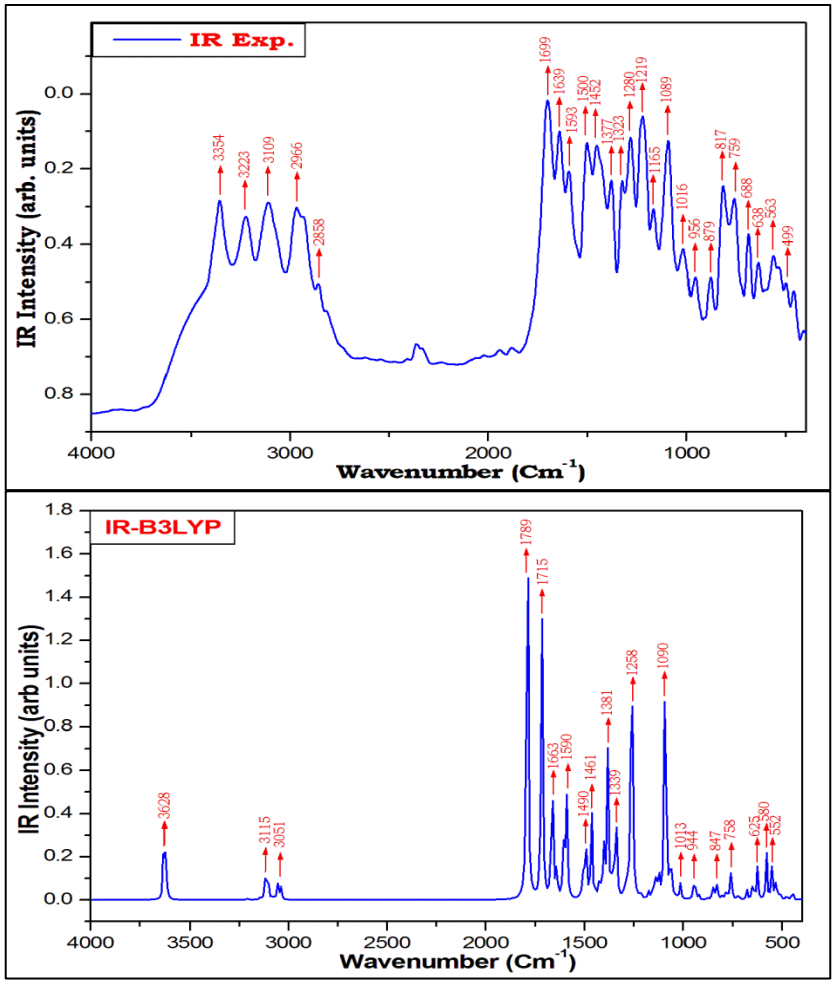

Figure 2 The experimental and theoretical FT-IR spectra of CNPC.

Table 2 The selected fundamental vibrational assignments of CNPC.

Mode No.	Calculated wavenumber		Observed wavenumber		Intensity		PED ≥ 10%
	Unscaled	Scaled	FT-IR	FT-Raman	IR	Raman	
1	3620	3501	3354		6.84	1.96	$\nu N_3H_4(99)$
2	3210	3104	3109		0.18	2.14	$\nu C_{14}H_{15}(95)$
3	3194	3089		3070	0.04	1.59	$\nu C_9H_{10}(96)+ \nu C_{11}H_{12}(98)$
4	3078	2976	2966		0.67	2.48	νC16H17(99)
5	3036	2936	2933	2934	2.24	8.36	νC29H30(99)+ νC29H31(98)+ νC29H32(98)
6	1789	1730	1699	1679	100.00	6.75	νO33C18(69)+ νN3C18(34)
7	1715	1659	1639	1635	56.86	12.96	νO1C25(85)
8	1663	1608	1593	1613	28.76	13.15	νC19C20(66)
9	1639	1585		1593	6.43	12.49	νC9C11(53)+ νC14C7(55)
10	1607	1554			9.26	3.98	νO36N34(80)+ νC13C14(58)+ νC7C8(43)
11	1591	1538	1500	1503	27.45	5.59	νO36N34(80)+ νO35N34(71)+ νC7C8(43)+βC8C9C11(49)
12	1505	1455	1452		5.23	0.28	βH10C9C8(75)+ βH12C11C13(68)+ βH15C14C13(74)+βC7C8C9(25)
13	1462	1414		1416	15.14	4.10	βH4N3C16(48)+ τC16C13C20H17(72)
14	1422	1375	1377	1375	3.70	1.97	βH22C21H24(66)+ βH22C21H23(74)
15	1358	1313	1323		6.66	1.25	νC14C7(55)+ βH17C16C13(63)
16	1339	1295	1280	1275	19.93	3.45	νC25C20(18)+ τC26H27C29H28(84)
17	1277	1235		1229	4.48	1.18	νN5C19(42)+ βH6N5C19(60)
18	1259	1217	1219	1205	67.71	4.59	νN3C18(34)+ τC16C13C20H17(72)
19	1214	1173	1165	1168	1.12	13.48	νC8C9(49)+ βC11C13C14(30)+ νC13C16(34)+ βH12C11C13(68)
20	1176	1137		1157	0.44	0.25	βH30C29C26(83)+ τC26C29O2H27(87)
21	1145	1107		1108	0.83	1.03	νC21C19(15)+ νN3C16(36)+ νC16C20(23)
22	1123	1086	1089	1089	6.16	1.77	τC29H30C26H31(65)
23	1061	1026		1023	9.27	7.51	νC37I8(48)+ βC8C9C11(49) + βC14C7C8(45)+ βC7C8C9(25)
24	1054	1019	1016		0.72	0.42	βH23C21H24(82)+ τC21H24C19H22(82)
25	1035	1001		1003	0.54	2.40	νC29C26(64)+ νO2C26(67)+ τC21H22C19H23(46)
26	985	953	956	963	0.03	0.10	ΓH10C9C11H12(78)+ ΓH12C11C13C16(88)
27	802	776		777	0.83	2.13	βC16N3C18(11)+ τO1C20O2C25(63)
28	785	759	759		1.36	2.19	τO36C7O35N34(60)+ τO1C20O2C25(63)
29	758	733		723	5.65	2.34	τO33N3N5C18(86)
30	653	631	638		2.16	3.56	βO1C25O2(40)
31	626	605		595	6.11	1.55	ΓC20C16C19N5(43)+ ΓC21C19C20C25(47)+ τC25C16C19C20(32)
32	581	562	563		8.64	1.92	βO35N34C7(26)+ ΓH4N3C18N5(77)+ ΓH6N5C19C21(79)
33	517	500	499		0.10	3.66	βC18N5C19(22)+ ΓH4N3C18N5(77)+ ΓH6N5C19C21(79)
34	349	337		338	1.28	1.10	βO35N34C7(26)+ βC20C19C21(58)+ βC7C8C37(65)
35	339	328		316	0.48	3.63	βC20C19C21(58)
36	247	239		238	0.63	1.81	βC16C20C25(42)+ ΓH32C29C26O2(83)

bending vibrations are computed at 297, 337 and 376 cm^{-1}, respectively.

NO_2 vibrations

The nitro stretching vibrations are the most characteristic bands in the spectra of nitro compounds, not only because of their spectral positions but also for their strong intensities. The nitro substituted aromatic compounds show asymmetric stretching mode in the region of 1600-1500 cm^{-1} and symmetric stretching mode in the region of 1385-1325 cm^{-1} [16]. In the present case, the asymmetric stretching vibrations of NO_2 are observed at 1500 cm^{-1}/FT-IR with medium intensity (27.45) and at 1502 cm^{-1}/FT-Raman spectrum. The calculated wavenumber at 1538 cm^{-1} is assigned for the asymmetric NO_2 vibrations. The symmetric stretching vibration of NO_2 is observed at 1323 cm^{-1} in FT-IR and calculated wavenumber computed at 1336 cm^{-1} with medium intensity. Aromatic nitro compounds show C–N stretching vibrations nearly ~870 cm^{-1} [16]. The theoretical band at 913 cm^{-1} is assigned for $\nu C_7–N_{34}$ vibration of the nitro group. The in-plane deformation of NO_2 is observed at 563 cm^{-1} in FT-IR and well agreed with the computed wavenumber at 562 cm^{-1}.

N–H and C– N vibrations

In heterocyclic molecules, the N–H stretching vibrations are usually appearing in the region of 3500-3300 cm^{-1} [17]. The band observed at 3354 cm^{-1} in FT-IR spectrum is assigned for the N-H stretching vibration. The $N_3–H_4$ and $N_5–H_6$ stretching modes of dihydropyrimidinone have been calculated at 3501 and 3509 cm^{-1}. The C-N stretching vibrations are normally occurring in the region 1400-1200 cm^{-1} [18]. The strong bands observed at 1229, 1205

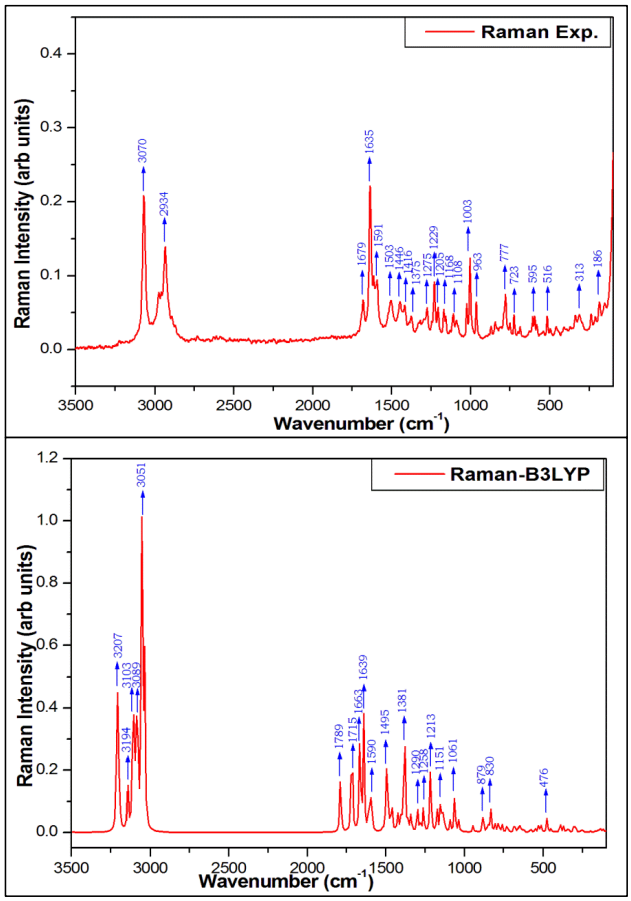

Figure 3 The experimental and theoretical FT-Raman spectra of CNPC.

cm^{-1} in FT-Raman and at 1219 cm^{-1} in FT-IR spectrum corresponds to the ν_{C-N} stretching vibrations of the title molecule. These bands are in good agreement with the calculated wavenumber at 1235 and 1217 cm^{-1}. The stretching wavenumber of C–N associated with bending vibrations of β_{CNH} and τ_{CCCC} vibrations. The bending vibrations of β_{CNH} are calculated at 1446, 1442, 1414 and 1395 cm^{-1}. Hence the corresponding experimental observation from FT-Raman shows wavenumber at 1446 and 1416 cm^{-1}.

C=O and C–O vibrations

The carbonyl stretching vibrations are normally occurs in the region 1715-1600 cm^{-1}, it is moderately active in Raman and intense in IR [19]. In the title molecule, the strong band observed at 1699 cm^{-1} in FT-IR with 100% IR intensity and 1679 cm^{-1} in FT-Raman is attributed to C=O stretching vibrations of dihydropyrimidine ring. The results of computation give the wavenumber of the corresponding mode at 1730 cm^{-1} has a contribution of 79% from C=O and minor contribution of 14% from C–N vibration. The C=O stretching vibration of ester group is observed at 1639 cm^{-1}/FT-IR and 1635 cm^{-1}/FT-Raman. The corresponding computed wavenumber for C=O is 1659 cm^{-1} and the deviation is attributed to intermolecular C=O dipole-dipole interaction in the molecule. The bands responses to the ester C–O stretching vibrations are occur in the region of 1260-1000 cm^{-1} [20]. These vibrations are intense and partly due to an interaction with C–C vibration. The strong band observed at 1089 cm^{-1} in FT-IR and 1089 cm^{-1} in FT-Raman assigned to ester C–O stretching vibrations. It is well agreed with calculated wavenumber at 1086 cm^{-1}.

C–H vibrations

The C–H stretching vibrations of aromatic ring absorb in its characteristic region 3100-3000 cm^{-1} [21]. The strong bands observed at 3109 cm^{-1} in FT-IR and 3070 cm^{-1} in FT-Raman confirms the C-H stretching vibrations of title molecule. The wavenumber computed at 3104, 3101 and 3089 cm^{-1} are well agreed with the experimental observations of C–H wavenumber. In the region below 3000 cm^{-1} are found aliphatic C–H stretching vibrations. The wavenumber corresponds to $\nu_{C16-H17}$ is observed as strong band at 2966 cm^{-1} in IR spectrum and its calculated wavenumber shows 2976 cm^{-1} with 99% of PED contribution. In substituted phenyl rings, the C–H in-plane bending vibrational modes can be expected in the region 1300-1000 cm^{-1} [22]. In our study, the β_{CCH} in-plane bending vibrations are computed at 1452, 1246, 1134 and 1113 cm^{-1}. The strong band observed at 1452 cm^{-1} in FT-IR represents the C–H in-plane bending vibration of the phenyl ring. The C–H out of plane bending vibrations is expected to occur in the region 1000-675 cm^{-1} [23]. The C–H out of plane bending vibration is observed as strong bands in both FT-IR and FT-Raman spectra at 956, 879, 817 and 963, 869 cm^{-1}, respectively. These spectral wavenumber agreed with the calculated wavenumber at 953, 892, 827 and 819 cm^{-1}.

Ring vibrations

The ring C–C stretching vibrations occur in the region 1625-1430 cm^{-1}. In the phenyl ring, the six carbon atoms undergo coupled vibrations called skeletal vibration [24,25]. In present investigation, the ring C–C stretching vibrations are observed as a strong band at 1593, 1503 cm^{-1} in FT-Raman and medium band at 1500 cm^{-1} in FT-IR are assigned for the ring vibrations. The theoretical wavenumber in the range 1585-1538 cm^{-1} represents the ring C–C vibrations. The strong bands at 1168 and 1023 cm^{-1} in FT-Raman and weak band at 1165 cm^{-1} in FT-IR outcomes the phenyl ring breathing and trigonal bending vibration of the title molecule. These fundamental wavenumber computed at 1173 and 1026 cm^{-1} represents the ring breathing and trigonal bending vibrations of aromatic ring system.

CH_3 and CH_2 group vibrations

In methyl groups, the symmetric stretching vibrations are observed lower wavenumber when compared to the asymmetric stretching vibrations of C-H bonds. The CH_3 symmetric vibrations are expected to occur in the range of 2950-2900 cm^{-1} and CH_3 asymmetric stretching vibrations are expected in the range 3050-2950 cm^{-1} [26,27]. The weak band observed at 2933 cm^{-1}/FT-IR and strong band at 2934 cm^{-1}/FT-Raman spectrum assigned for the symmetric stretching vibrations of the methyl group present in the carboxylate side chain. This mode has been calculated at 2936 cm^{-1}. The symmetric C–H vibrations of methyl and methylene group of CNPC calculated at 2955 and 2950 cm^{-1}. The asymmetric vibrations of the methyl and methylene groups of title molecule computed in the region 3039-2987 cm^{-1}. In many molecules, the symmetric deformations CH_3 appears with an

intensity varying from medium to strong and expected in the range 1380 ± 25 cm^{-1} [26]. This band has been observed at 1377 cm^{-1} in the FT-IR spectrum and 1375 cm^{-1} in FT-Raman spectrum. The rocking vibrations of methyl group usually observed in the region 1100 ± 95 cm^{-1} [28]. In present case, the medium band observed at 1016 cm^{-1} in FT-IR denotes the rocking vibration of methyl group attached to dihydropyrimidine rind and its corresponding computed wavenumber at 1019 cm^{-1}. The rocking mode for the methyl group present in the carboxylate side chain shows weak band at 1157 cm^{-1} in FT-Raman spectrum and its calculated wavenumber at 1137 cm^{-1}.

NBO Analysis

The molecular interactions occur in both the occupied and unoccupied molecular orbitals are examined by the Natural bond orbital analysis. Second order perturbation theory analysis of Fock matrix in NBO basis of CNPC is tabulated in **Table 3**. From the NBO results, two main orbital interactions are observed in the nitro group of the title molecule. The strong intra-molecular hyperconjugative interaction of $LP(O_{35})\rightarrow\pi^*N_{34}-O_{36}$ which increases the ED(0.5941) that weakens the respective anti-bonds leading to highest stabilization of 636.55 kJ/mol. From the **Table 3**, the stabilizing energy of $n(LP3O_{35})\rightarrow\sigma^*(C_7-N_{34})$, $(N_{34}-O_{36})$ and $n(LP3O_{36})\rightarrow\sigma^*(C_7-N_{34})$, $(N_{34}-O_{35})$ correspond to 52.17, 76.82 and 53.72, 80.92 kJ/mol, respectively. The strong intra-molecular hyperconjugative interaction of π(C–C)→π*(C–C) bonds of the phenyl ring increases ED at the six conjugated π-bonds. From the NBO analysis, the π-electron delocalization in phenyl ring revealed by the ED at the three conjugated π-bond (≈1.63-1.67e) and π*(≈0.30-0.45e) resulting to the stabilization energies of ≈69.54-96.99 kJ/mol, respectively. The π-electron cloud movement can make the molecule highly polarized and causes internal charge transfer, which is responsible for the activity of the title molecule. The orbital overlap between n(Cl)→π*(C-C) bond orbital, which increases ED(0.4526) that weakens the respective anti-bonds (C7–C8=1.398Å) when compared to other C-C bonds of the phenyl ring leading to the stabilization of 62.38 kJ/mol. The most important interactions are $n(LP2)O_1\rightarrow\sigma^*O_2-C_{25}$, $n(LP2)O_2\rightarrow\pi^*O_1-C_{25}$, $n(LP1)N_3\rightarrow\pi^*C_{18}-O_{33}$, $n(LP1)N_5\rightarrow\pi^*(C_{18}-O_{33})$, $(C_{19}-C_{20})$ and $n(LP2)O_{33}\rightarrow\sigma^*N_5-C_{18}$ provides stabilization energy of about 130.46, 185.94, 185.27, 160.92, 169.83 and 109.24 kJ/mol, respectively. The orbital occupancies of donor, acceptor and donor-acceptor interactions are visualized with the help of Chemcraft 1.8 software. The donor-acceptor interaction orbitals of CNPC were shown in **Figure 4**. These types of interactions are responsible for the pharmaceutical and biological activity of the title molecule.

NLO Optics

Nonlinear optical studies is at the forefront of current research

Table 3 The donor-acceptor interactions in NBO basis for CNPC.

Type	Donor	ED/e	Acceptor	ED/e	[a]E(2) kJ/mol	[b]E(j)-E(i) a.u	[c]F(i,j) a.u
π -π*	C7-C8	1.6767	C9-C11	0.3025	69.54	0.32	0.065
π -π*			C13-C14	0.3247	79.66	0.32	0.069
π -π*			N34-O36	0.5941	58.16	0.18	0.047
π -π*	C9-C11	1.6405	C7-C8	0.4526	96.99	0.25	0.07
π -π*			C13-C14	0.3247	81.09	0.29	0.067
π -σ*	C13-C14	1.6381	N3-C16	0.0285	8.24	0.6	0.034
π -π*			C7-C8	0.4526	93.89	0.26	0.069
π -π*			C9-C11	0.3025	87.4	0.29	0.07
π -π*	C19-C20	1.8423	O1-C25	0.3047	97.11	0.29	0.076
n -σ*	LP(2) O1	1.8548	O2-C25	0.0958	130.46	0.62	0.126
n -σ*			C20-C25	0.0558	66.73	0.72	0.098
n -σ*	LP(1) O2	1.9637	O1-C25	0.0183	29.04	1.16	0.081
n -π*	LP(2) O2	1.8048	O1-C25	0.3047	185.94	0.33	0.112
n -σ*	LP(1) N3	1.7345	C13-C16	0.0456	30.17	0.65	0.065
n -σ*			C16-H17	0.0232	12.76	0.67	0.043
n -σ*			C18-O33	0.0439	10.46	0.83	0.043
n -π*			C18-O33	0.3284	185.27	0.33	0.11
n -π*	LP(1) N5	1.6803	C18-O33	0.3284	160.92	0.34	0.103
n -π*			C19-C20	0.2326	169.83	0.31	0.103
n -σ*	LP(2) O33	1.8465	N3-C18	0.0717	98.49	0.71	0.118
n -σ*			N5-C18	0.0860	109.24	0.65	0.118
n -σ*	LP(2) O35	1.8970	C7-N34	0.1027	52.17	0.55	0.074
n -π*			N34-O36	0.0629	76.82	0.72	0.104
n -σ*	LP(3) O35	1.4357	N34-O35	0.0683	25.52	0.7	0.067
n -π*			N34-O36	0.5941	636.55	0.16	0.141
n -σ*	LP(2) O36	1.8941	C7-N34	0.1027	53.72	0.55	0.075
n -σ*			N34-O35	0.0683	80.92	0.71	0.106
n -π*	LP(3) Cl37	1.9142	C7-C8	0.4526	62.38	0.31	0.067

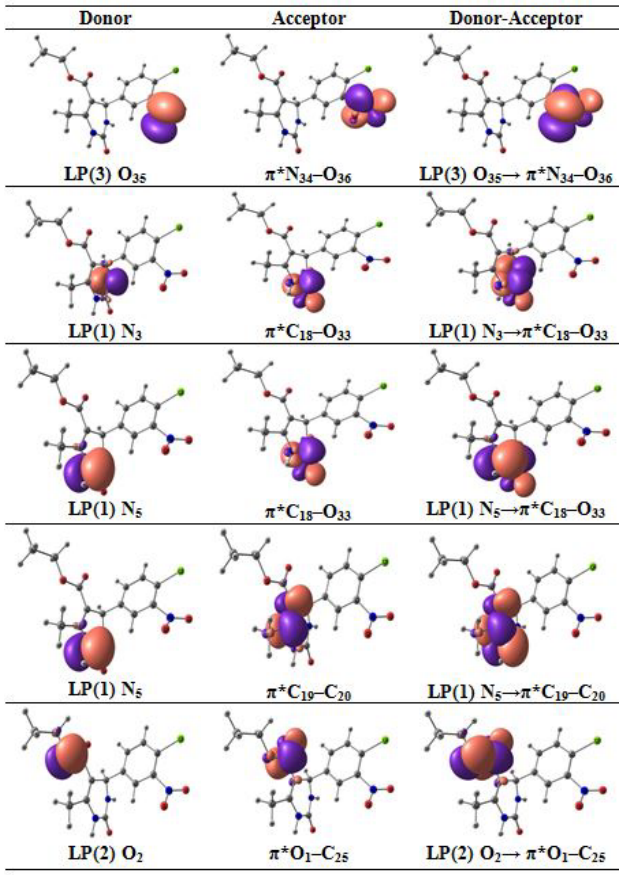

Figure 4 The donor-acceptor interaction orbitals of CNPC.

because of its prominence in providing the key functions of optical switching, optical modulation, optical logic and optical memory for the emerging technologies in areas such as signal processing, telecommunications and optical interconnections [29,30]. The molecular polarizability and hyperpolarizability are calculated about 4.71×10^{-30} esu and 2.61×10^{-30} esu, respectively. The β_0 value of the title compound is seven times greater than that of reference urea. Urea is one of the prototypical molecules used in the study of the NLO properties of molecular systems. Therefore, it was used frequently as a threshold value for comparative purposes [31]. The first hyperpolarizability values of similar pyrimidine derivatives are reported as, 1.19, 1.35 and 0.30×10^{-30} esu, respectively [32-34]. The first hyperpolarizability components of CNPC were listed in **Table 4**.

Molecular Electrostatic Potential

Molecular electrostatic potential is related to the electronic density of the molecule and is a very useful descriptor in understanding the charge sites as well as hydrogen bonding interactions [35,36]. The electrostatic potential *V*(r) are also well suited for analyzing processes based on the ''recognition'' of one molecule by another, as in drug-receptor, and enzyme substrate interactions, because it is through their potentials that the two species first ''see'' each other [37,38]. Being a real physical property *V*(r)s can be determined experimentally by diffraction or by computational methods [39]. The MEP mapped surface

Table 4 The first hyperpolarizability components of CNPC

Parameters	B3LYP/6-31G(d,p)
Dipole moment (μ)	Debye
μ_x	2.5812
μ_y	-1.1982
μ_z	-0.1884
μ	2.8519 Debye
Polarizability (α_0)	$\times 10^{-30}$esu
α_{xx}	246.60
α_{xy}	8.27
α_{yy}	239.80
α_{xz}	1.66
α_{yz}	21.69
α_{zz}	177.97
α	4.7147×10^{-30}*esu*
Hyperpolarizability (β_0)	$\times 10^{-30}$esu
β_{xxx}	-12.65
β_{xxy}	11.97
β_{xyy}	248.19
β_{yyy}	-372.31
β_{xxz}	-34.20
β_{xyz}	-12.66
β_{yyz}	37.17
β_{xzz}	-97.30
β_{yzz}	94.09
β_{zzz}	-42.64
β_0	2.6143×10^{-30}esu

*Reference urea (μ=1.3732 Debye, β_0=0.3728 × 10^{-30} esu)

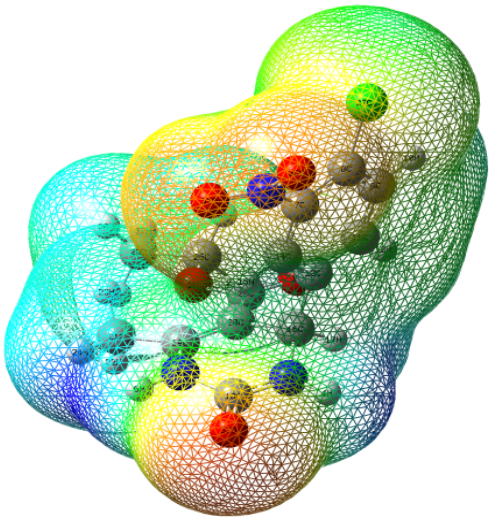

Figure 5 The molecular electrostatic potential mapped surface of CNPC.

and 2D contour map of CNPC were shown in **Figure 5**. In order to predict the possible electrophilic and nucleophilic charge sites for the investigated molecule, MEP mapped surfaces are

generated. The positive (blue) regions to nucleophilic reactivity and the negative (red and yellow) regions of MEP were related to electrophilic reactivity shown in **Figure 5**. The negative potentials are commonly observed in the region of electronegative atoms with lone pair electrons. In our study, the negative regions are localized in the oxygen atoms present in the nitro group and also with the oxygen atoms present in the two carbonyl groups, which are electrophilic nature. The positive potentials are localized over the hydrogen atoms bonded with the nitrogen atoms of dihydropyrimidinone ring, which are nucleophilic in nature.

Energy Gap Analysis

Frontier molecular orbitals and their energies are very useful for the physicists and chemists. The analysis of the wave function indicates that the electron absorption corresponds to the transition from the ground to the first excited state and is mainly described by one-electron excitation from the highest occupied molecular orbital (HOMO) to the lowest unoccupied orbital (LUMO). The eigen values of HOMO/LUMO and their energy gap reflect the chemical activity of the molecule. In order to gain insight into the electronic structure of CNPC, it's theoretical molecular orbital distributions were calculated with the Gaussian program at B3LYP/6-31G(d,p) level using the density functional theory. As shown in the **Figure 6** the highest occupied molecular orbitals of CNPC were mostly dispersed on the 4-chloro-3-nitrophenyl moiety. In contrast, the LUMO were localized on the electron deficient pyrimidine ring together with the carboxylate side chain. The clear separation of the HOMO and LUMO suggested that the HOMO-LUMO excitation would shift the electron density distributions from the donor di-substituted phenyl moiety to the acceptor pyrimidine moiety leading to a polarized excited state. The contour map of title molecule describes the electron density mapped surface of the CNPC. It is more important, such separation of HOMO-LUMO can provide holes and electron-transporting channel, respectively.

HOMO=-6.8682 eV

LUMO=-2.7783 eV

Energy gap ΔE=4.0899 Ev

NMR Analysis

Gauge independent atomic orbital method is used as a default method to calculate the NMR chemical shifts of the CNPC molecule. The recorded ^{1}H-NMR and ^{13}C-NMR spectra of the CNPC molecule are shown in **Figure 7**. **Table 5**, contains the assignments of experimental and theoretical chemical shift values of the title compound. The GIAO-NMR calculations were performed by B3LYP/6-31G(d,p) level of theory. Chemical shift of any 'x' proton (δX) is equal to the difference between isotropic magnetic shielding (IMS) of TMS and proton (x). It is defined by the equation: δX=IMSTMS–IMSX [40]. The theoretical NMR chemical shifts repositioned using proper scale factors. The ^{1}H-NMR chemical shifts of CNPC (with respect to TMS) appeared in the range of 1.014-9.250 ppm experimentally and 0.862-7.456 ppm theoretically. The triplet and singlet observed at 1.037 and 2.225 ppm corresponds to the two methyl protons of the title molecule. These chemical shifts are in good accordance with the theoretical values at 1.064 and 2.373 ppm, respectively. The confirmation of the compound formation is observed by the singlet at 5.110 ppm in ^{1}H-NMR chemical shift shows good agreement with the peak computed at 4.820 ppm. The quartet observed at the range of 3.354-3.988 ppm corresponds to the methylene group protons of the title molecule. Theoretical chemical shift for methylene group is computed in the range of 3.584-3.667 ppm, respectively. The experimental aromatic protons show nice accordance with the theoretical values.

In ^{13}C-NMR spectrum the fourteen signals confirms the fourteen carbons of the title molecule experimentally in the range of 13.95-165.10 ppm and theoretically at 12.04-169.06 ppm, respectively. The signal observed at 53.17 ppm confirms the ring formation chiral carbon of the title molecule; its theoretical prediction coincides well with 56.47 ppm. The two signals 165.10 and 156.67 ppm at downfield region confirms the two carbonyl carbons (C_{25} and C_{18}) of the CNPC molecule. These carbonyl carbon signals computed at 164.00 and 146.96 ppm. The peaks appeared at 13.95, 17.65 and 59.11 corresponds to the two methyl and one methylene carbon of the CNPC molecule. The calculated data of these carbons are 12.04, 21.14 and 60.95 ppm, respectively.

Conclusion

Nonlinear organic molecule ethyl-4-(4-chloro-3-nitrophenyl)-6-methyl-2-oxo-1,2,3,4-tetrahydropyrimidine-5-carboxylate has synthesized and characterized using spectral techniques. The stable conformer was identified with the relative energy of about -1542.44631 Hatree. Using potential energy distribution the vibrational modes of the recorded wavenumbers were assigned. The NBO analysis reveals the strong hyperconjugative interactions occur in the molecule leads to the stabilization of the molecular system. The small energy gap value 4.0899 eV is responsible for the nonlinear activity of the investigated molecule. The first hyperpolarizability calculated as 2.6143 x 10-30 esu, which is

Table 5 The theoretical and experimental chemical shift values of CNPC.

^{13}C-NMR			^{1}H-NMR		
Atoms	DFT	Exp.	Atoms	DFT	EXP.
C29	12.04	13.95	$-C_{29}H_3$	0.862-1.064	1.014-1.061
C21	21.14	17.69	$-C_{21}H_3$	0.838-2.373	2.225
C16	56.47	53.17	$-C_{26}H_2$	3.584-3.667	3.918-3.988
C26	60.95	59.19	H17	4.820	5.11
C14	125.14	117.30	ArC–H	6.814-7.456	6.943-7.411
C20	100.50	98.76	N–H	3.886	7.781
C8	134.99	119.81	N–H	5.008	9.250
C11	132.01	122.84			
C9	129.50	130.19			
C13	145.39	142.27			
C7	150.94	148.77			
C19	146.31	151.89			
C18	146.96	156.64			
C25	164.06	165.10			

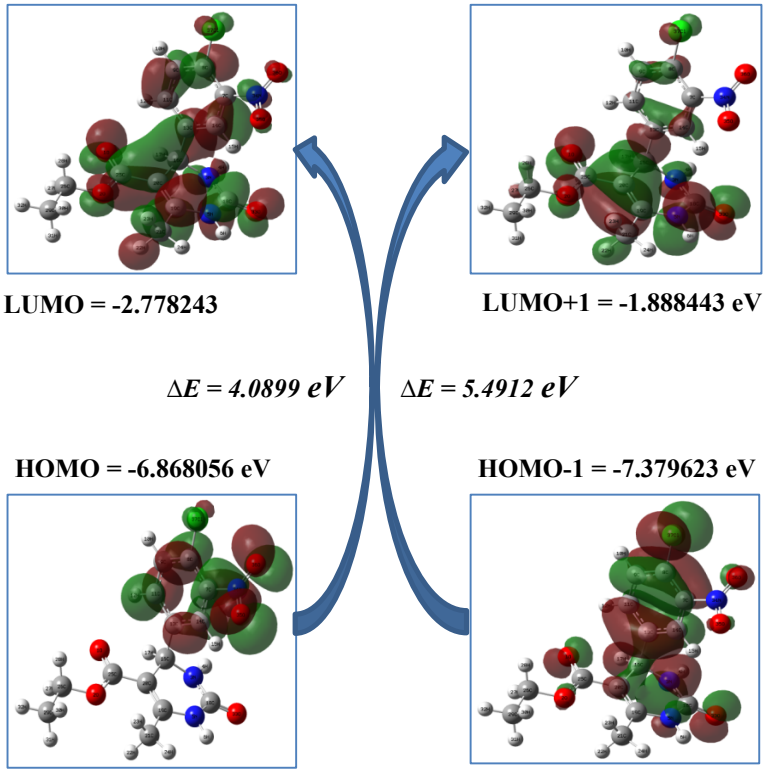

Figure 6 The frontier molecular orbitals of CNPC.

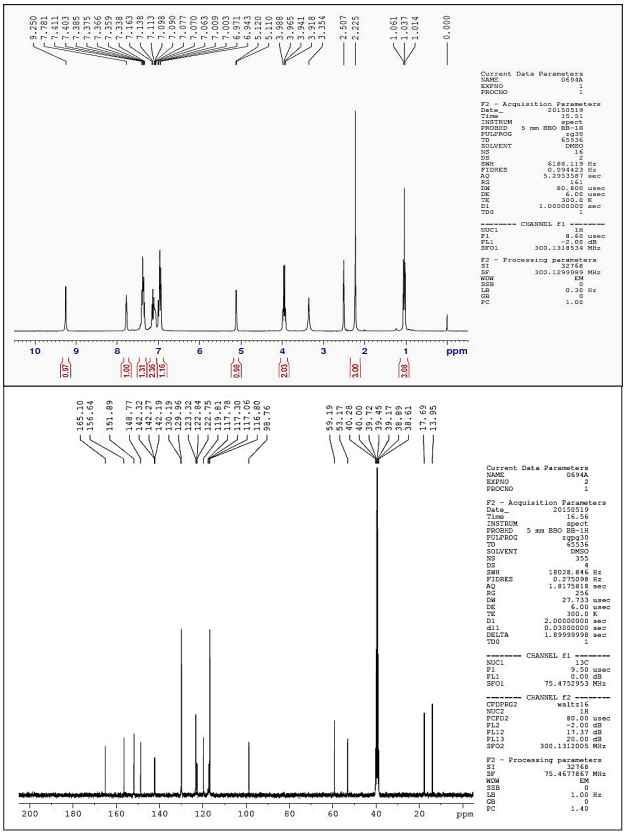

Figure 7 The ^{1}H and ^{13}C-NMR spectra of CNPC.

seven times greater than that of reference urea and their similar NLO molecules. Thus our title molecule is good candidate for the nonlinear optical studies. The molecular charge sites are identified by the molecular electrostatic potential mapped surface. The structural confirmation by ^{1}H and ^{13}C-NMR reports with computed chemical shifts shown very good agreement.

References

1 Chemla DS, Zyss J (1987) In Nonlinear Optical Properties of Organic Molecules and Crystals, Academic Press: New York.

2 Nalwa SH (2008) In Handbook of Organic Electronics and Photonics, American Scientific Publishers: Los Angeles.

3 Mutter L, Koechlin M, Jazbinsek M, Gunter P (2007) Direct electron beam writing of channel waveguides in nonlinear optical organic crystals. Opt Expr 15: 16828-16838.

4 Hwang EJ, Cheong CS, Lee H, Lee SW, Kim IT, Lee SH (2005) Synthesis and Photoluminescent Properties of Violet Emitting 5,6-Diphenylfuro[2,3-d]pyrimidine Derivatives. ChemInform 36: 47.

5 Weng J, Mei Q, Fan Q, Ling Q, Tong B, Huang W (2013) Bipolar luminescent materials containing pyrimidine terminals: synthesis, photophysical properties and a theoretical study. RSC Adv 3: 21877-21887.

6 Lin LY, Tsai CH, Wong KT, Huang TW, Wu CC, et al. (2011) Efficient organic DSSC sensitizers bearing an electron-deficient pyrimidine as an effective π-spacer J Mater Chem 21: 5950-5958.

7 Achelle S, Rodríguez-López J, Cabon N, Guen FR (2015) Protonable pyrimidine derivative for white light emission RSC Adv 5: 107396-107399.

8 Cui LS, Liu Y, Liu XY, Jiang ZQ, Liao LS (2015) Design and Synthesis of Pyrimidine-Based Iridium(III) Complexes with Horizontal Orientation for Orange and White Phosphorescent OLEDs ACS Appl Mater Interfaces 7: 11007-11014.

9 Gaussian 03 (2004) Revision C.02, Gaussian Inc., Wallingford, CT.

10 Jamroz MH (2004) Vibrational Energy Distribution Analysis: VEDA4 program, Warsaw, Poland.

11 Michalska D (2003) Raint Program, Wroclaw University of Technology.

12 Michalska D, Wysokinski R (2005) The prediction of Raman spectra of platinum(II) anticancer drugs by density functional theory Chem. Phys. Lett., 403:211-217.

13 Doddamani SB, Ramoji A, yenagi J, Tonamavar J (2007) The vibrational spectra, assignments and ab initio/DFT analysis for 3-chloro, 4-chloro and 5-chloro-2-methylphenyl isocyanates Spectrochim acta A 67:150-159.

14 Socrates G (1981) IR characteristics group frequencies, John Wiley, New York.

15 Roeges NPG (1994) A guide to complete interpretation of IR spectra of organic compounds, Wiley, New York.

16 Barthes M, DeNunzio G, Ribet G (1996) Polarons or proton transfer in chains of peptide groups? Synth Met 76: 337-340.

17 Socrates G (2001) Infrared and Raman characteristic group frequencies – Tables and Charts, (3rd edn), Wiley, Chichester.

18 Dhandapani A, Manivarman S, Subashchandrabose S, Saleem H (2014) Molecular structure and vibrational analysis on (E)-1-(3-methyl-2,6-diphenyl piperidin-4-ylidene) semicarbazide. J Mol Struct 1058: 41-50

19 Dhandapani A, Manivarman S, Subashchandrabose S (2016) Synthesis, single crystal structure, Hirshfeld surface and theoretical investigations on pyrimidine derivative. Chem Phys Lett 655-656: 17-29.

20 Lin-Vein D, Colthup NB, Fateley WG, Grasselli JG (1991) The Hand Book of Infrared and Raman Characteristic Frequencies of Organic Molecules, Academic Press, San Diego.

21 Varsanyi G (1969) Vibrational Spectra of Benzene Derivatives, Academic Press, New York.

22 Silverstein RM, Clayton Bessseler G (1976) Spectroscopic Identification of organic compounds, Wiley, New York.

23 Mohan J (2001) Organic Spectroscopy: Principles and Applications, (2nd edn), Narosa Publishing House, New Delhi.

24 Bellamy LJ (1975) The Infrared Spectra of Complex Molecules, John Wiley & Sons, Inc, New York.

25 Coates J (2000) in RA Meyers (Ed.), Interpretation of Infrared Spectra, A Practical Approach, John Wiley and Sons Ltd, Chichester.

26 Colthup NB, Daly LH, Wiberly SE (1990) Introduction to Infrared and Raman Spectroscopy, (3rd edn), Academic Press, Boston.

27 Dollish FR, Fateley WG, Bentley FF (1997) Characteristic Raman Frequencies of Organic Compounds, John Wiley and Sons, New York.

28 Nakano M, Fujita H, Takahata M, Yamaguchi K (2001) Theoretical Study on Second Hyperpolarizabilities of Phenylacetylene Dendrimer: Toward an Understanding of Structure−Property Relation in NLO Responses of Fractal Antenna Dendrimers. J Am Chem Soc 124: 9648-9655.

29 Tanak H (2011) DFT computational modelling studies on 4-(2,3-Dihydroxybenzylideneamino)-3-methyl-1H-1,2,4-triazol-5(4H)-one. Comput Theoret Chem 967: 93-101.

30 Ozdemir M, Sonmez M, Sen F, Dinçer M, Ozdemir N (2015) A novel one-pot synthesis of heterocyclic compound (4-benzoyl-5-phenyl-2-(pyridin-2-yl)-3,3a-dihydropyrazolo[1,5-c]pyrimidin-7(6H)-one): Structural (X-ray and DFT) and spectroscopic (FT-IR, NMR, UV-Vis and Mass) characterization Studies Spectrochim. Acta A 137: 1304-1314.

31 Al-Abdullah ES, Mary YS, Panicker CY, El-Brollosy NR, El-Emam AA, et al. (2014) Theoretical investigations on the molecular structure, vibrational spectra, HOMO–LUMO analyses and NBO study of 1-[(Cyclopropylmethoxy)methyl]-5-ethyl-6-(4-methylbenzyl)-1,2,3,4-tetrahydropyrimidine-2,4-dione. Spectrochim acta A 133: 639-650.

32 Panicker CY, Varghese HT, Eapen PE, Raju K, Ganguli S, et al. (2010) Spectroscopic investigations of 2-hydroxy-4-methyl pyrimidine hydrochloride. Int J Chem Sci 8: 655-662.

33 Pir H, Günay N, Tamer Ö, Avcı D, Atalay Y (2013) Theoretical investigation of 5-(2-Acetoxyethyl)-6-methylpyrimidin-2,4-dione: Conformational study, NBO and NLO analysis, molecular structure and NMR spectra. Spectrochim acta A 112: 331-342.

34 Scrocco E, Tomasi J (1978) Electronic Molecular Structure, Reactivity and Intermolecular Forces: An Euristic Interpretation by Means of Electrostatic Molecular Potentials. Adv Quant Chem 11: 115-193.

35 Luque FJ, Lopez JM, Orozco M (2000) Perspective on Electrostatic interactions of a solute with a continuum. A direct utilization of ab initio molecular potentials for the prevision of solvent effects. Theor Chem Acc 103: 343-345.

36 Politzer P, Laurence PR, Jayasuriya K, McKinney J (1985) Molecular electrostatic potentials: an effective tool for the elucidation of biochemical phenomena Health Perspect. 61: 191-202.

37 Scrocco E, Tomasi J (1973) The electrostatic molecular potential as a tool for the interpretation of molecular properties Topics in Current Chemistry. Springer 7:95-170.

38 Tanak H, Alaman AA, Büyükgüngör O (2013) Combined experimental and DFT computational studies on (E)-1-(5-nitrothiophen-2-yl)-N-[4-(trifluoromethyl)phenyl] methanimine. J Mol Struct 1048: 41-50.

39 Singh RN, Verma D, Kumar A, Baboo V (2012) Synthesis, molecular structure and spectral analysis of ethyl 4-[(3,5-dinitrobenzoyl)-hydrazonomethyl]-3,5-dimethyl-1H-pyrrole-2-carboxylate: A combined experimental and quantum chemical approach. Spectrochim Acta Part A 88: 60-71.

40 Konstantinov IA, Broadbelt LJ (2011) Regression Formulas for Density Functional Theory Calculated ^{1}H and ^{13}C NMR Chemical Shifts in Toluene-d8J. Phys Chem C 115: 12364-12372.